



PII S0025-5408(96)00040-2

NON-STOICHIOMETRY AND STRUCTURE OF MOLYBDENUM DISELENIDE

Haruo Naruke, Noboru Wakatsuki, Yoshihiro Hoshi, and Yoshinori Sasaki
Department of Applied Chemistry, Faculty of Engineering, Chiba University,
Yayoi-cho, Inage-ku, Chiba 263, Japan

(Refereed)

(Received December 13, 1995; Accepted February 26, 1996)

ABSTRACT

Molybdenum diselenides were synthesized at 1273 K for 24 h. The X-ray diffraction (XRD) analysis showed the compound to be non-stoichiometric in the approximate range of $1.85 \leq \text{Se/Mo} \leq 2.0$. Density measurements suggested a co-existence of interstitial Mo and Se vacancies in the lattice over the non-stoichiometric range. Well-grown crystals of hexagonal 2Hb-type were formed in the range of $1.9 \leq \text{Se/Mo} \leq 2.0$, whereas fine powders were given for $\text{Se/Mo} < 1.9$. In the latter range, a mixed-stacking of 2Hb- and 3R-type layers was suggested to take place, and the ratio of 2Hb:3R in the compounds of $\text{Se/Mo} = 1.85$ was estimated to be about 85:15 by means of a simulation of the XRD patterns. Compressed samples of $1.85 \leq \text{Se/Mo} < 1.9$ were higher in the electrical conductivity and were smaller in its temperature dependence, compared with those of $1.9 \leq \text{Se/Mo} \leq 2.0$.

KEYWORDS: A. chalcogenides, A. inorganic compounds, C. X-ray diffraction, D. crystal structure

INTRODUCTION

Molybdenum diselenide, MoSe_2 , which is a layer compound isomorphous with MoS_2 , has been studied so far concerning methods of single crystal growth (1,2), crystal structures (3), electrical and optical properties (4-6). For the last several decades, interests have also been focused on an application of MoSe_2 and MoS_2 to materials for conversion of sunlight into electrical energy in a photoelectrochemical cell (7). Although the stoichiometric MoSe_2 has been characterized well as described above, little is known concerning its non-

stoichiometry. Spiesser *et al.* (8) have reported a range of non-stoichiometry of MoSe_2 to be $1.9 \leq \text{Se/Mo} \leq 2.0$, and concluded that the non-stoichiometry involves only Se vacancies.

In the present study, the non-stoichiometry of MoSe_2 was characterized by means of a composition analysis, X-ray diffraction analysis, density measurement, and the measurement of electrical conductivity. Some of the results were not in agreement with those of Spiesser *et al.*, especially with respect to the defect structure in the non-stoichiometric range. The present paper also describes a new phase having a composition range of $1.85 \leq \text{Se/Mo} < 1.9$, in which the compound possesses a stacking disorder of Se–Mo–Se sheets.

EXPERIMENTAL

Sample Preparation. Elemental molybdenum (99.9 wt%, particle size: 3 μm) and selenium (99.999 wt%) were weighed at a molar ratio of $\text{Se/Mo} = 1.8\text{--}2.0$, and mixed thoroughly in an agate mortar. The mixture was put in a quartz tube (inner diameter: 8 mm), which was evacuated to 10^{-2} Torr (1.33 Pa) by a rotary-pump, then filled to 1 atm with argon gas purified by having been passed through heated active copper and phosphorus pentoxide, and finally re-evacuated. This evacuating and filling were repeated for three or four times. Finally, the tube was sealed under reduced pressure. The resulting ampoule was heated in a furnace at 1273 ± 5 K for 24 h, and then cooled at room temperature.

Analysis and Measurement. The Se/Mo ratio of a sample was analyzed as follows. The sample was fired in air at 773 K for 12 h, giving MoO_3 . The Mo content of the sample was determined from the weight of MoO_3 formed. The Se content was estimated by subtraction of the Mo weight from the initial weight of the sample. Results are listed in Table 1, in which the analyzed Se/Mo ratios mostly agree with the initial mixing ratios. It should be noticed, however, that every Se/Mo ratio has an error range of ± 0.03 , which is estimated from Table 1. In the following, we have used Se/Mo values as the initial mixing ratios.

Scanning electron microscopic (SEM) images of the sample were taken with the Topcon ABT-32T Scanning Electron Microscope. X-ray diffraction (XRD) patterns were measured on a diffractometer (MAC science, MPX-18 system) at 298 K using CuK_α radiation. Systematic errors of the diffraction angles were corrected by an internal standard, $\alpha\text{-Al}_2\text{O}_3$ (rhombohedral, $a = 4.7588$, $c = 12.992$ Å (9)), and by the factors estimated by Wilson (10)

TABLE I
Compositions of Molybdenum Selenide

Mixing Se/Mo	Analyzed Se/Mo
1.85	1.88
1.88	1.91
1.90	1.91
1.93	1.93
1.95	1.94
2.00	2.01

and Pike (11). Lattice constants were refined for the corrected angles using least-squares technique.

The density of a sample was measured hydrostatically using a pycnometer. About 2 g of the sample was put in the pycnometer (volume: ca. 5 cm³) and immersed in kerosene. The pycnometer containing the sample and kerosene was evacuated until bubbles on the surface of the sample and the inner wall of the pycnometer were removed completely. The density of the stoichiometric MoSe₂ was determined to be 6.95 ± 0.02 gcm⁻³, which is in good agreement with the theoretical value (6.97 gcm⁻³), demonstrating a reliability of this method.

The sample was ground in the mortar and compressed (pressure: ca. 2.5 × 10³ kg cm⁻²) into a pellet with a diameter of 0.5 cm (i.e., area: 0.196 cm²). After the thickness of the pellet (*d* cm) was measured, an electro-conductive resin (Fujikura Kasei, D-500) was fixed on both circles of the pellet as electrodes. The resistance (*R* Ω) between the electrodes was measured on the digital multimeter (Keithley, 196 SYSTEM DMM). There was little change in resistance when several values of current, ranging from 0.5 to 50 μA, were supplied on the sample. The electrical conductivity (σ S cm⁻¹) was given by $\sigma = 0.196/(R \cdot d)$. As measurements were performed for the compressed powders which had not been sintered, it should be remarked that the resulting data may not be dominated by intrinsic property but governed by interparticle contacts. Temperature of the sample (*T* K) was altered from ca. 190 K to 303 K at the heating rate of 2 or 3 Kmin⁻¹ using a temperature controller (Ohkura Electric, EC-5500). Since the XRD pattern of the compressed surface of the pellet for Se/Mo = 2.0 showed this surface to have a preferred orientation parallel to (00*l*) plane, conductivity was also measured parallel to this surface to check an anisotropy of the conductivity. But no considerable anisotropy could be observed.

RESULTS

The samples of 1.9 ≤ Se/Mo ≤ 2.0 were crystalline compounds having metallic luster, whereas the samples of Se/Mo < 1.9 were gray-black fine powders. The SEM images are represented in Figure 1. The samples of Se/Mo = 1.9 and 2.0 are well-grown crystals having a shape of hexagonal plate with the diameters of about 100 μm. Although the crystals of Se/Mo = 1.85 are also hexagonal in shape, their crystal sizes are only around 1–5 μm as shown in Fig. 1(c) and 1(d).

Figure 2 shows the XRD patterns for several Se/Mo ratios. The relative intensities of diffraction peaks from the (00*l*) planes in Figure 2(a) and 2(b) are large due to a preferred orientation of the plate-shaped crystals. All of the diffraction angles in patterns (a), (b), (c), and (d) in Figure 2 except 2θ = 26.0° (*d* = 3.42 Å) are in agreement with the literature values of hexagonal MoSe₂ (12) (Fig. 2(f)). The peak at 2θ = 26.0° can be assigned to rhombohedral MoSe₂, which will be shown later. Since the weak peak at 2θ = 40.5° (*d* = 2.22 Å) in Figure 2(e) can be assigned to a small excess of metallic Mo, the range of non-stoichiometry at 1273 K is concluded to be 1.85 ≤ Se/Mo ≤ 2.0. It is noticeable that the widths of (10*l*) lines in Fig. 2(c) and 2(d) are significantly larger than those of (*h*00) and (00*l*) lines. The refined lattice constants shown in Figure 3 are almost independent of the composition.



FIG. 1

Scanning electron microscopic images of molybdenum selenide: (a) $\text{Se}/\text{Mo} = 2.0$; (b) $\text{Se}/\text{Mo} = 1.95$; (c) and (d) $\text{Se}/\text{Mo} = 1.85$.

The composition dependence of the density is represented in Figure 4. In this figure, the theoretical curves related to three types of defects are also plotted with broken lines: (a) Mo at interstitial positions in the lattice; (b) both interstitial Mo and vacancies of Se at the same concentration; (c) vacancies of Se. The refined unit cell volume was used for calculation of the theoretical density. The observed density, being almost constant in the non-stoichiometric range, supports an existence of the defect type (b).

Plots of $\log \sigma$ against $1/T$ are shown in Figure 5. All of the plots exhibit semiconductive properties. In the range of $\text{Se}/\text{Mo} < 1.9$, σ was higher and the temperature dependence of σ was smaller than those in the range of $1.9 \leq \text{Se}/\text{Mo} \leq 2.0$. The thermal activation energies of σ were estimated through the least-squares fitting on these plots, resulting in 0.31–0.35 eV for $1.9 \leq \text{Se}/\text{Mo} \leq 2.0$ and 0.08–0.11 eV for $1.85 \leq \text{Se}/\text{Mo} < 1.9$.

DISCUSSION

MoSe_2 is a layer compound which is isomorphous with MoS_2 (3). Sheets of Se–Mo–Se sandwiches are stacked each other in the direction of the hexagonal *c*-axis. A sheet interacts with the adjacent one through the Se...Se van der Waals force. Within a sheet, each Mo

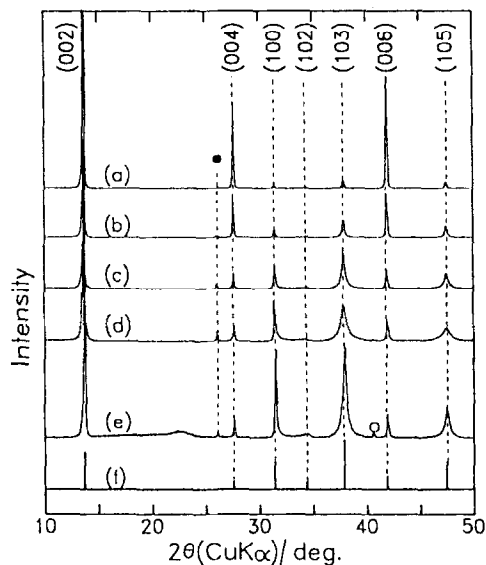


FIG. 2

X-ray diffraction patterns of molybdenum selenide: (a) Se/Mo = 2.0; (b) Se/Mo = 1.95; (c) Se/Mo = 1.88; (d) Se/Mo = 1.85; (e) Se/Mo = 1.8; (f) the reference data of 2Hb-MoSe₂ (13). Closed circle represents 3R-MoSe₂ (14); open circle represents Mo metal.

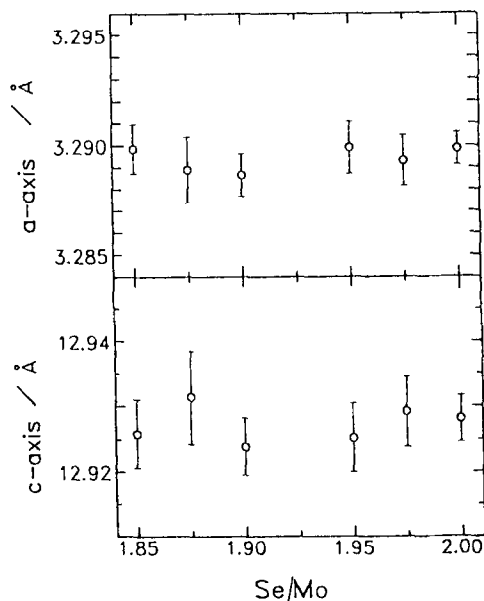


FIG. 3

Composition dependence of lattice constants of molybdenum selenide.

atom is surrounded by six Se atoms with the trigonal prismatic coordination. Two types of stacking of sheets have been known for MoSe₂, namely, 2Hb- (3,12) and 3R-type (13). A unit cell of 2Hb-type contains two Se-Mo-Se sheets, whereas that of 3R-type contains three sheets.

From the XRD analysis, the non-stoichiometric range was estimated to be $1.85 \leq \text{Se/Mo} \leq 2.0$. From the point of view of the difference in the crystal size, XRD profile, and electrical conductivity, this homogeneous range seems to be divided into two parts: $1.85 \leq \text{Se/Mo} < 1.9$ and $1.9 \leq \text{Se/Mo} \leq 2.0$. In the following, these two composition ranges will be discussed.

1.9 \leq Se/Mo \leq 2.0. The composition dependence of density (Fig. 4) indicated the co-existence of interstitial Mo atoms and Se vacancies in almost the same concentration. This is different from the results of Spiesser et al. (8), who observed a decrease in density with a decrease of Se/Mo ratio, and concluded that the non-stoichiometry of MoSe₂ arises from only Se vacancies. However, the density data reported by them are smaller than the theoretical values by about 0.2 gcm⁻³ over the range of $1.9 \leq \text{Se/Mo} \leq 2.0$.

For instance, the density of MoSe₂ that they observed (Fig. 1 in ref. 8) can be read as c.a. 6.72 gcm⁻³, whereas the theoretical density is 6.97 gcm⁻³ (12). This deviation from the theoretical value is not negligible, because the density of 6.72 gcm⁻³ corresponds to a

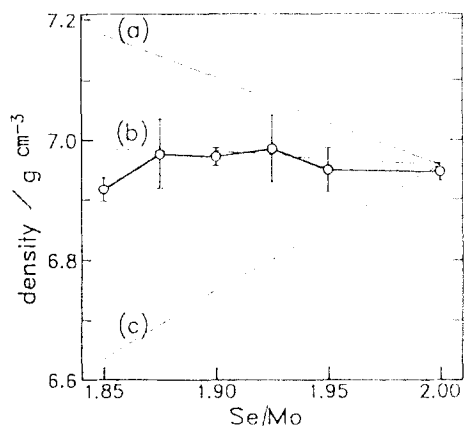


FIG. 4

Composition dependence of density of molybdenum selenide. Broken lines are theoretical densities related to the three types of the lattice defects, (a) interstitial Mo, (b) interstitial Mo and Se vacancies in the same concentration, and (c) Se vacancies.

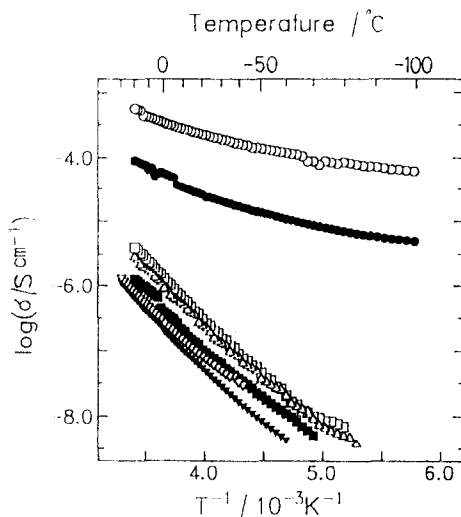


FIG. 5

Temperature dependence of conductivity of molybdenum selenide: \blacktriangledown Se/Mo = 2.0, \triangle Se/Mo = 1.98, \blacksquare Se/Mo = 1.95, \square Se/Mo = 1.9, \bullet Se/Mo = 1.88, \circ Se/Mo = 1.85, and ∇ Se/Mo = 2.0, measured parallel to the compressed surface of the pellet.

composition of Se/Mo = 1.88, which is calculated from the unit cell volume of MoSe₂ (12). ZrSe_x ($x = 1.85$ – 1.95) (14) is one example of metal dichalcogenides exhibiting non-stoichiometry that involves lattice defects of both interstitial metal atoms and Se vacancies. In this case, the occurrence of substitutions of Se with Zr has been speculated (14). Although there is no information on the location of the interstitial Mo in this study, almost the same concentration of the defects of the two types over the homogeneous range implies an interaction between the sites of the two defect types.

In the case of ZrSe_x (14), *c*-axis of the hexagonal lattice increased by about 0.02 Å with a change of *x* from 1.95 to 1.85. It seems curious that the size of the unit cell of MoSe₂ was almost constant over the non-stoichiometric range (Fig. 3). However, insertions of additive atoms into some metal dichalcogenides do not give rise to an increase in their *c*-axis, as revealed for Al_xTaS₂, AlNbSe₂ (15), and Ta_{1+x}S₂ (16).

It is observed that conductivities and their thermal activation energies are almost independent of the composition, suggesting that the lattice defects give little effect on the electrical properties. At present we have no reasonable explanation for this problem. For further discussion of this behavior, information on the electrical properties of single crystals and on the detailed defect structure is required. A scanning tunneling microscopic (STM) measurement on these crystals may be suitable for this purpose, because this measurement provides information on both atomic arrangements and band structures.

$1.85 \leq \text{Se/Mo} < 1.9$. In this composition range, a co-existence of interstitial Mo and Se vacancies was suggested from the density measurement (Fig. 4).

In the XRD patterns of $\text{Se/Mo} = 1.85$ and 1.88 (Fig. 2(c) and 2(d)), the line widths of $(10l)$ diffractions were significantly large. It has been reported that hexagonal close-packed crystals having a stacking disorder give broad diffraction patterns except $h-k = 0 \pm 3n$, where n is an integer (17). On the other hand, XRD patterns similar to Fig. 2(c) and 2(d) have been observed for $\text{Re}_x\text{Ta}_{1-x}\text{Se}_2$ in which 2Hb- and 3R-type layers are stacked randomly (18). Furthermore, the peak at $2\theta = 26.0^\circ$ ($d = 3.42 \text{ \AA}$) in Figure 2(b) and 2(c) has been observed for 3R-MoSe₂ ($d = 3.43 \text{ \AA}$) (13)). On the assumption that the line broadening of the $(10l)$ diffraction is due to the mixed-stacking of 2Hb and 3R-type layers, the ratio of 2Hb: 3R was estimated for $\text{Se/Mo} = 1.85$ through a simulation of XRD patterns using a model of Hayashi et al. (18). First, the 2Hb- and 3R-type layers, which contain two and three Se-Mo-Se sheets, respectively, were constructed. Atomic positions within the 2Hb layer (hexagonal lattice) for Mo are $(1/3, 2/3, 1/4)$, $(2/3, 1/3, 3/4)$ and for Se are $(2/3, 1/3, 1/8)$, $(2/3, 1/3, 3/8)$, $(1/3, 2/3, 5/8)$, $(1/3, 2/3, 7/8)$; and within the 3R layer (hexagonal lattice) for Mo are $(1/3, 2/3, 1/6)$, $(0, 0, 1/2)$, $(2/3, 1/3, 5/6)$ and for Se are $(2/3, 1/3, 1/12)$, $(2/3, 1/3, 1/4)$, $(1/3, 2/3, 5/12)$, $(1/3, 2/3, 7/12)$, $(0, 0, 3/4)$, $(0, 0, 11/12)$. Their unit cell sizes are $a = 3.296$, $c = 6.464 \times 2 \text{ \AA}$ for 2Hb and $a = 3.296$, $c = 6.464 \times 3 \text{ \AA}$ for 3R. Then the 2Hb and 3R layers were stacked randomly to form a unit cell for simulation. The resultant unit cell consisted of 300 Se-Mo-Se sheets, and was $a = 3.296$, $c = 6.464 \times 300 \text{ \AA}$ in size. The lattice defects of interstitial Mo and Se vacancies were not introduced to this model because of their negligible influence to the diffraction intensities. The calculation of diffraction patterns was made for several 2Hb:3R ratios. The polarization and Lorentz factors were taken into account, and thermal parameters were fixed at 1.0. The results are displayed in Figure 6(a),

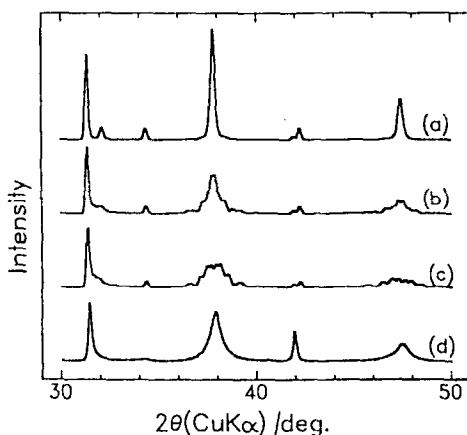


FIG. 6

X-ray diffraction patterns of molybdenum selenide. Computed patterns (a) mixed-layer structure having 95% 2Hb and 5% 3R layers, (b) mixed-layer structure having 85% 2Hb and 15% 3R layers, and (c) mixed-layer structure having 75% 2Hb and 25% 3R layers. Observed pattern (d) of $\text{Se/Mo} = 1.85$. Relatively high intensity for the (006) line at $2\theta = 42.0^\circ$ is due to the preferred orientation of the crystals.

(b), and (c). The profiles and line widths of the (103) and (105) diffractions in the observed pattern of $\text{Se}/\text{Mo} = 1.85$ (Fig. 6(d)) agrees well with the pattern calculated for 2Hb: 3R = 85:15 (Fig. 6(b)). Since the 3R-type MoSe_2 can be prepared only at high-temperatures and high-pressures (for example, 1973 K, 4.7×10^9 Pa (19)), it is of interest that 3R structure is formed under the conditions in this study. A small amount of 3R-type MoSe_2 was also found when crystals of 2Hb-type MoSe_2 were grown by means of a chemical transport technique using Br as a transport agent (5). In this case, however, the mixed-stacking of 2Hb- and 3R-type layers does not take place, because no systematic broadening of diffraction lines has been observed (5). The random stacking of 2Hb and 3R layers, as well as the defects of interstitial Mo and Se vacancies, disturbs the periodicity of the crystal lattice and inhibits the growth of crystals, resulting in the small size of the crystals (Fig. 1(c) and 1(d)).

In this composition range, the conductivities were higher and the temperature dependence was smaller than for $1.9 \leq \text{Se}/\text{Mo} \leq 2.0$. The formation of 3R-type suggested above has little effect on the conduction properties, because the electronic structure of 3R-type is similar to that of 2Hb-type (20). Our qualitative measurement of thermoelectric powers showed the sample of $\text{Se}/\text{Mo} = 1.85$ to be a n-type semiconductor, indicating that the conduction properties are caused by donor levels within the band gap of MoSe_2 .

CONCLUSIONS

Molybdenum diselenides were synthesized at 1273 K for 24 h. The non-stoichiometric range was estimated to be $1.85 \leq \text{Se}/\text{Mo} \leq 2.0$ from the XRD analysis. The existence of both interstitial Mo and Se vacancies in the lattice was suggested in the range of $1.9 \leq \text{Se}/\text{Mo} \leq 2.0$. A broadening of the XRD lines was observed in the compositions of $\text{Se}/\text{Mo} < 1.9$. A mixed-stacking of the 2Hb- and 3R-type layers was assumed and the ratio of 2Hb:3R for $\text{Se}/\text{Mo} = 1.85$ was estimated to be about 85:15 by means of a simulation of XRD patterns. Compressed samples of $\text{Se}/\text{Mo} < 1.9$ were higher in the electrical conductivity and were smaller in temperature dependence, compared with those of $1.9 \leq \text{Se}/\text{Mo} \leq 2.0$.

REFERENCES

1. A.A. Al-Hilli and B.L. Evans, *J. Cryst. Growth*, **15**, 93 (1972).
2. F. Lévy, *Nuovo Cimento* **38**, 359 (1977).
3. K.D. Bronsema, J.L. de Boer, and F. Jellinek, *Z. Anorg. Allg. Chem.* **540/541**, 15 (1986).
4. S.H. El-Mahalawy and B.L. Evans, *Phys. Stat. Sol. (b)* **79**, 713 (1977).
5. B.L. Evans and R.A. Hazelwood, *Phys. Stat. Sol. (a)* **4**, 181 (1971).
6. K.K. Kam and B.A. Parkinson, *J. Phys. Chem.* **86**, 463 (1982).
7. See for example: H. Tributsch, *Ber. Bunsenges. Phys. Chem.* **81**, 361 (1977); F.-R.F. Fan, H.S. White, B. Wheeler, and A.J. Bard, *J. Electrochem. Soc.* **127**, 518 (1980); L.F. Schneemeyer, M.S. Wrighton, A. Stacy, and M.J. Sienko, *Appl. Phys. Lett.* **36**, 701 (1980).
8. M. Spiesser, J. Rouxel, M. Kerriou, and M.G. Goureaux, *Bull. Soc. Chim. Fr.* **5**, 1427 (1969).
9. JCPDS X-Ray Powder Data File, card 42-1468.
10. A.J.C. Wilson, *J. Sci. Instrum.* **27**, 321 (1950).
11. E.R. Pike, *J. Sci. Instrum.* **34**, 355 (1957).
12. JCPDS X-ray Powder Data File, card 29-914.
13. M.S. Silverman, *Inorg. Chem.* **6**, 1063 (1967).

14. A. Gleizes and Y. Jeannin, *J. Solid State Chem.* 1, 180 (1970).
15. J.M. van den Berg Voorhoeve, *J. Less-Common Met.* 26, 399 (1972).
16. F. Jellinek, *J. Less-Common Met.* 4, 9 (1962).
17. S. Lele, T.R. Anantharaman, and Ch.A. Johnson, *Phys. Stat. Sol.* 20, 59 (1967).
18. K. Hayashi, T. Ikeuchi, H. Takeuchi, and M. Shimakawa, *J. Alloys Comp.* 219, 161 (1995).
19. JCPDS X-ray Powder Data File, card 20-757.
20. N.J. Doran, *Physica* 99B, 227 (1980).